ACS Biomaterials SCIENCE & ENGINEERING

pubs.acs.org/journal/abseba

Article

Inserting Menthoxytriazine into Poly(ethylene terephthalate) for Inhibiting Microbial Adhesion

Pengfei Zhang, Jiyu Li, Mei Yang, Lifei Huang, Fanqiang Bu, Zixu Xie, Guofeng Li, and Xing Wang*

Cite This: https://doi.org/10.1021/acsbiomaterials.1c01448

Read Online

ACCESS | Metrics & More | Article Recommendations | Supporting Information

ABSTRACT: Antimicrobial modification of poly(ethylene terephthalate) (PET) is effective in preventing the adhesion and growth of microorganisms on its surface. However, few methods are available to modify PET directly at its backbone to impart the antimicrobial effect. Herein, menthoxytriazine-modified PET (PMETM) based on the stereochemical antimicrobial strategy was reported. This novel PET was prepared by inserting menthoxytriazine into the PET backbone. The antibacterial adhesion test and the antifungal landing test were employed to confirm the antiadhesion ability of PMETM. PMETM could effectively inhibit the adhesion of bacteria, with inhibition ratios of 99.9 and 99.7% against *Escherichia coli* (Gram-negative) and *Bacillus subtilis* (Gram-positive), respectively. In addition, PMETM exhibited excellent resistance to *Aspergillus niger* (fungal) contamination for more than 30 days. Cytotoxicity assays indicated that PMETM was a noncytotoxic material. These results suggested that the insertion of menthoxytriazine in the PET backbone was a promising strategy to confer antimicrobial properties to PET.

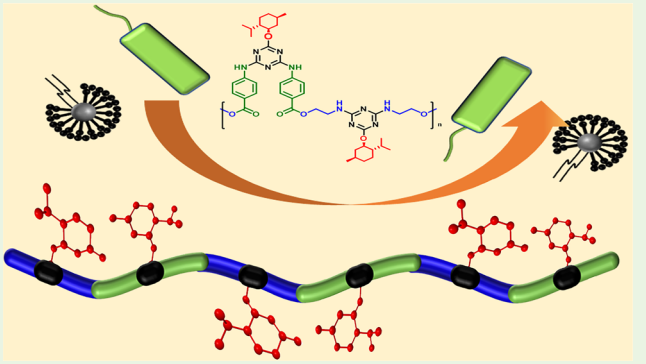

KEYWORDS: *antimicrobial adhesion, menthol, PET, stereochemistry, triazine*

1. INTRODUCTION

Poly(ethylene terephthalate) (PET) has been used in a wide range of applications due to its unique properties such as easy processing, good biocompatibility, and stable physical and chemical properties.[1−4] However, PET-based products often provide a "hotbed" for the growth of harmful microorganisms because of their poor antimicrobial properties.[5] As human healthcare awareness has increased, there is great concern about the range of serious consequences caused by PET products, such as hospital- and device-associated infections caused by biofilms formed by pathogenic bacteria on implants and medical devices.[6−10] Therefore, it is urgent to develop new antimicrobial PET materials.

Much effort has been made to develop antimicrobial PET. Many studies have demonstrated that organic or inorganic antimicrobial agents could be introduced into PET by compounding, coating, or grafting to endow it with good antimicrobial properties.[11−16] Ping et al. prepared a hybrid film by immobilizing nanosilver on the surface of acrylic grafted PET.[5] Antibacterial experiments showed that this film has strong and stable bactericidal efficiency against *Escherichia coli*. Zhang et al. prepared quaternary ammonium salt and nanosilver-modified antibacterial PET by electron beam irradiation, and this modification greatly enhanced the antibacterial efficiency of PET.[14] However, these strategies may increase the risk of bacterial resistance and cause potential cellular and environmental toxicity.[17−20] Nongrafting strategies may fail to achieve long-lasting antimicrobial effects due to the release of antimicrobial substances. In addition, the accumulation of dead bacteria on the surface of the material may not only reduce bactericidal activity but also cause an immune response and inflammation, leading to more serious problems.[21−24] Therefore, a new strategy is urgently needed to introduce the antimicrobial modification of PET.

In recent years, stereochemical strategies have received special attention because of their safe, nontoxic, nonrelease, and long-term advantages.[25−28] The theoretical basis of this antibacterial strategy is the selective recognition by microorganisms of chiral terpenoid molecules (borneol or menthol).[29−31] The chiral terpenoid molecule-grafted surfaces and polymers exhibited excellent antimicrobial (bacterial and fungal) properties.[24−27] The related studies have shown that the antimicrobial adhesion performance based on stereochemistry is closely related to the number of grafted chiral molecules,[32,33] indicating that the increase of the modification

Received: November 14, 2021
Accepted: December 16, 2021

Scheme 1. Synthesis Processes of PMETM[a]

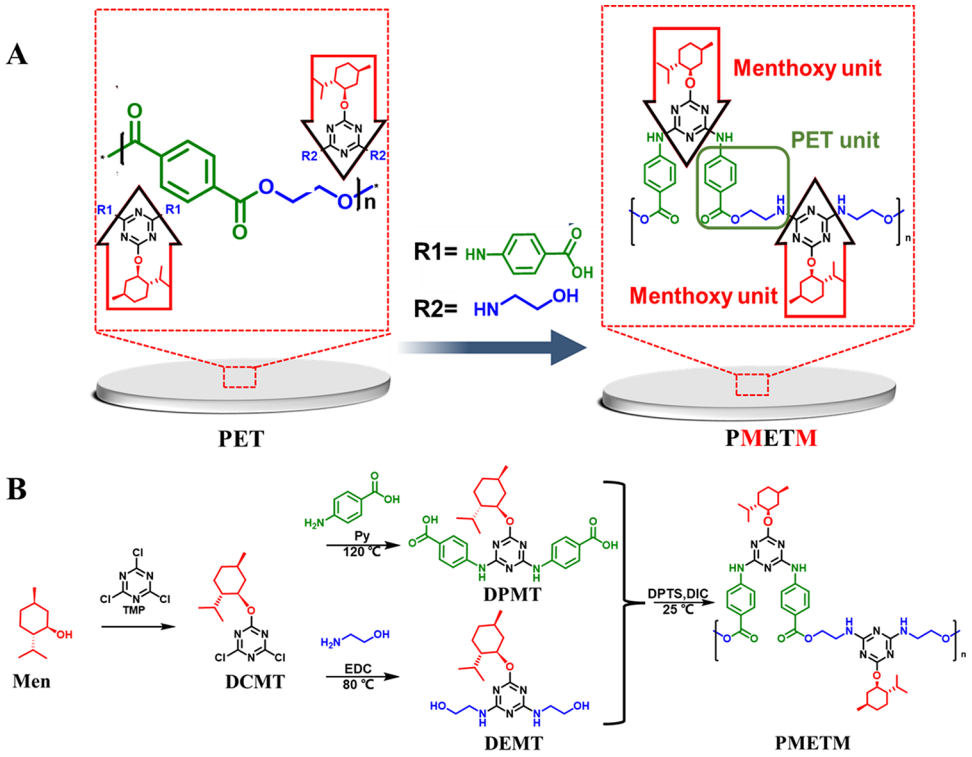

[a](A) Schematic diagram of the PET modification strategy and (B) synthesis processes of PMETM from menthol.

density of stereochemical terpene molecules will help to improve the antimicrobial adhesion properties of modified PET. Menthol is a typical terpenoid molecule whose modified materials have emerged as candidates for antimicrobial adhesion.[34,35] Compared with borneol, menthol is more likely to produce various derivatives due to its low spatial resistance and high reactivity.[36,37] Therefore, skeleton modification of PET with the menthol moiety should be an appropriate method to impart antimicrobial adhesion properties to PET. Triazine has been used as a suitable carrier for polymer synthesis because it can be replaced by different amine nucleophiles to produce triazine derivatives with different numbers of substitutions, depending on the reaction temperature.[38] Based on the above foundation, it would be promising to design antimicrobial PET by inserting the menthoxytriazine block into the main chain.

Herein, double menthoxytriazine-modified PET (PMETM) was reported. As shown in Scheme 1A, double menthoxy groups were inserted into the PET backbone via the polymerization of 2-menthol-4,6-ethanolamine-1,3,5-triazine (DEMT) and 2-menthol-4,6-aminobenzoic-1,3,5-triazine (DPMT). The antibacterial adhesion test (including the antibacterial spreading test and the plate counting test) and the antifungal landing test were employed to investigate the antiadhesion ability of PMETM against *Escherichia coli* (Gram-negative), *Bacillus subtilis* (Gram-positive), and *Aspergillus niger* (fungus), respectively. In addition, the cytotoxicity of PMETM was also investigated by 3-(4,5-dimethylthiazol-2-yl)-2,5-diphenyltetrazolium bromide (MTT) and the LIVE/DEAD cell viability assay.

2. EXPERIMENTAL SECTION

2.1. Materials. PET was purchased from Guangdong Chemical Factory (Guangdong, China). L-Menthol, 2,4,6-trihylpyridine, terephthalic acid (TA), 4-aminobenzoic (PABA), diisopropylcarbodiimide (DIC), malt extract agar, tryptone soy agar (TSA), and trypticase soy broth (TSB) were all purchased from Aladdin. Pyridine and ethanolamine were purchased from Macklin. 1,3,5-Triazine was purchased from J&K Scientific. 4-(Dimethylamino)pyridinium-4-toluenesulfonate (DPTS) was prepared according to literature methods.[39] All of the chemicals were used as received without any purification. All of the solvents were purchased from Tianjin Da Mao Chemical Reagent Factory. A LIVE/DEAD cell viability assay kit was obtained from Thermo Fisher Scientific Co. *E. coli* (ATCC 25922), *B. subtilis* (ATCC 9372), *A. niger* (CICC 41254), were obtained from the China Center of Industrial Culture Collection. Mouse fibroblast cells (L929) were obtained from Cell Resource Center, IBMS, CAMS/PIMC, Beijing, China.

2.2. Synthesis of 2-Menthol-1,3,5-triazine (DCMT). Briefly, L-menthol (9.36 g, 0.06 mmol) was added to 20 mL of dichloromethane (DCM) and mixed by magnetic stirrer until dissolved completely. After adding 1,3,5-triazine (5.53 g, 0.03 mmol) and 2,4,6-trimethylpyridine (4 mL, 0.04 mmol), the mixture was mixed for another 12 h at 0 °C. Afterward, the mixture was washed three times with deionized water. Then, the organic phase was filtered and placed on a rotary evaporator to remove excess DCM. Further purification was performed by silica gel column chromatography (200−300 mesh, Sinopharm Chemical Reagent Co., Ltd., China; eluents were petroleum ether/DCM = 5:1). A white solid was obtained in 80% yield.

2.3. Synthesis of 2-Menthol-4,6-ethanolamine-1,3,5-triazine (DEMT). In a typical synthesis process, DCMT (1.82 g, 0.006 mmol) was added to 20 mL of 1,2-dichloroethane and mixed by magnetic stirring until dissolved completely. After adding ethanolamine (3.66 g, 0.06 mmol), the mixture was refluxed for 8 h at 80 °C. Afterward, the mixture was washed three times with deionized water. Then, the organic phase was filtered and placed on a rotary evaporator

https://doi.org/10.1021/acsbiomaterials.1c01448
ACS Biomater. Sci. Eng. XXXX, XXX, XXX−XXX

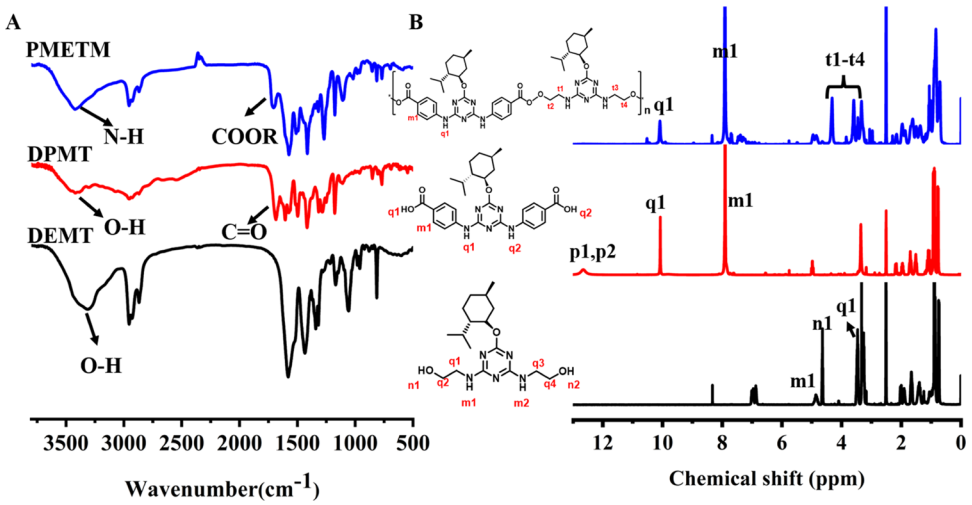

Figure 1. Characterization of DPMT, DEMT, and PMETM: (A) FTIR spectra. (B) ^{1}H NMR spectra.

to remove excess solvent, affording the desired product as a white powder in 80% yield.

2.4. Synthesis of 2-Menthol-4,6-PABA-1,3,5-triazine (DPMT). In a typical synthesis process, DCMT (1.82 g, 0.006 mol) was added to 20 mL of dimethylformamide (DMF) and mixed by magnetic stirring until dissolved completely. After adding PABA (4.11 g, 0.03 mol) and pyridine (0.23 g, 0.003 mol) slowly, the mixture was refluxed for 6 h at 150 °C. After the temperature decreased to room temperature, the mixture was washed three times with hot deionized water. Afterward, the mixture was acidified with diluted hydrochloric acid solution to pH = 3, and a light yellow powder was obtained by pumping, filtration, and drying under vacuum in 70% yield.

2.5. Synthesis of PMETM. In a typical experiment, DEMT (0.50 g, 2 mmol), DPMT (0.50 g, 2 mmol), and DPTS (0.003 g, 0.5 mmol) were charged into a N_2-filled reaction flask. DCM (2 mL) was then added and stirred until the monomer was dissolved in the solvent. Next, DIC (1.5 mL, 1.5 mmol) was added to the reaction in an ice water bath. The temperature was maintained at 0 °C for 1.5 h, the ice water bath was removed, and the mixture continued to react for 24 h at room temperature. Afterward, the crude product was dissolved in a minimum of DCM and precipitated in cold methanol. The final product was obtained after vacuum drying at 60 °C as a yellow powder in 75% yield.

2.6. Characterization. ^{1}H NMR spectra of the monomers and polyester were recorded on a Bruker AV-500 spectrometer using dimethyl sulfoxide (DMSO) as a solvent and tetramethylsilane (TMS) as the internal reference. Fourier transform infrared (FTIR) spectra of the polymer were recorded on a Nicolet Avatar-360 using KBr pellets. Gel permeation chromatography (GPC) measurements were carried out with an Agilent instrument (model 1100). Water was used as the eluent at a flow rate of 1 mL/min, and the column oven was set at 25 °C.

2.7. Bacterial Antiadhesion Assays. According to the previously reported method, the bacterial antiadhesion assays of menthol-derived polyester were studied by the antibacterial spreading test.[40] PMETM powder was pressed into regular pellets (diameter = 13 mm, thickness = 0.75 mm), and PET pellets were used as a control for the same test. Two pellets were placed on beef extract peptone medium, and then two small round aseptic media were placed on the discs to form a sandwich structure. Then, 2 μL of *E. coli* or *B. subtilis* suspension prepared in advance (the detailed preparation method can be referred to the literature[40]) was dropped on each of the small round media and cultured at 37 °C. The experimental phenomena were recorded by taking photographs at intervals.

Classical plate count assays and optical density (OD) tests were used to quantitatively assess the antibacterial adhesion properties of PMETM with slight modifications based on previous reports.[33] Sterilized PMETM sheets were first immersed in 1 mL of *E. coli* or *B. subtilis* suspension (10^6 CFU/mL) for 24 h. Then, the material was gently rinsed three times with sterile water to remove the floating bacteria from the surface. Next, the material was submerged in 2 mL of sterile saline and sonicated using an ultrasonic cleaner (50 W, 10 min) to disperse the bacteria strongly adhering to the surface of the material in saline. Then, 0.1 mL of the dilution was applied to TSA medium and incubated at 37 °C for 24 h. The results of bacterial growth were recorded with a camera. The antibacterial adhesion rate of PMETM compared to PET was calculated using the following equation

$$\text{antibacterial adhesion rate } (\%) = (A - B)/A \times 100$$

where A and B are the colony-forming units (CFUs) of raw PET and PMETM, respectively.

For OD testing, after a gentle rinsing step, PMETM sheets were placed in 50 mL of sterile liquid Luria–Bertani (LB) medium and incubated at 37 °C with shaking (200 rpm). The growth curves of *E. coli* or *B. subtilis* were obtained by monitoring the change in OD at 600 nm at different intervals (3, 6, 9, 12, 15, 18, 21, 24, and 27 h).

2.8. Fungal Antiadhesion Assays. According to the previously reported method, the antifungal behavior of PMETM was investigated by the fungal landing test.[41] PMETM powder was pressed into regular pellets (diameter = 13 mm, thickness = 0.75 mm), and PET pellets were used as a control for the same test. The material was immobilized separately on the surface of wort agar medium. Then, 10 μL of the pre-prepared black fungal suspension (detailed preparation can be found in the literature[41]) was dropped into the center of the plate with a distance of about 15 mm from the pellets. Finally, the medium was placed in a fungal incubator at 30 °C, and photographs were taken at regular intervals to record the experimental phenomena.

2.9. Cytotoxicity Evaluation. The cytotoxicity of PMETM was evaluated with L929 mouse fibroblasts. Briefly, 0.2 g of PET or PMETM was sterilized under ultraviolet light and immersed in 2 mL of 1640 medium for 24 h. The extract was used as a complete cell medium after the addition of 10% fetal bovine serum (FBS), 100 units/mL penicillin, and 100 μg/mL streptomycin. L929 mouse fibroblast cells were cultured in the conditioned medium at 37 °C in a humidified environment of 95% air and 5% CO_2. After 48 h of incubation, cell viability was determined by the MTT assay kit. The relative growth rate (RGR) of the cells was calculated by RGR (%) = Abs_{490} sample/Abs_{490} control × 100, where Abs_{490} sample and Abs_{490} control are the absorbance of the samples and the reference at 490 nm, respectively.

In addition, the LIVE/DEAD cell viability assay was also used to observe the viability of the cells after treatment with polymeric extracts. After 48 h of incubation, the cells were washed twice with PBS. Under light-proof conditions, 50 μL of LIVE/DEAD staining

https://doi.org/10.1021/acsbiomaterials.1c01448
ACS Biomater. Sci. Eng. XXXX, XXX, XXX−XXX

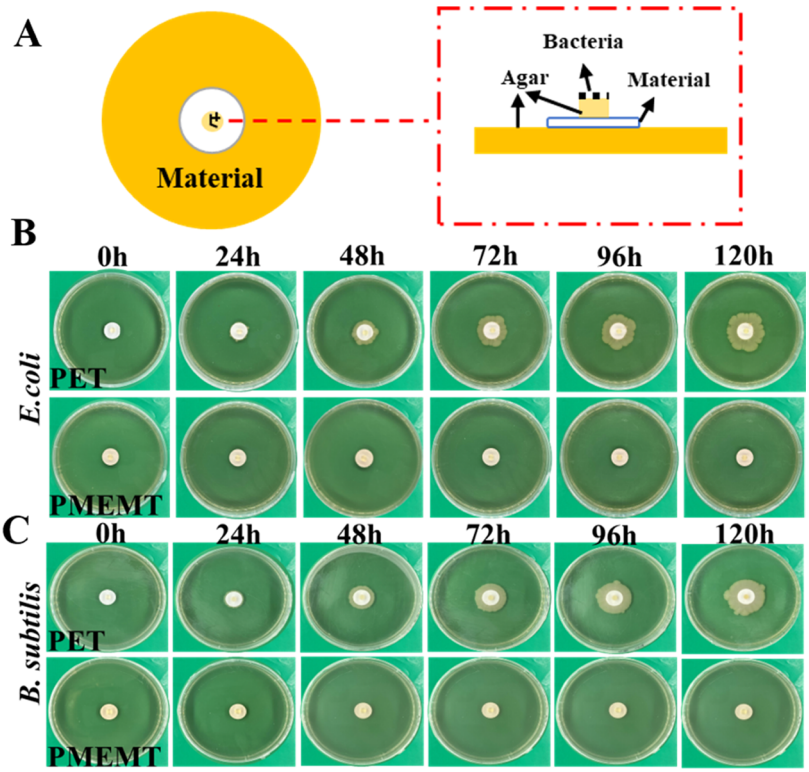

Figure 2. Antibacterial spreading test of PMETM. (A) Schematic illustration of the antibacterial spreading test model. (B) Digital photographs of the antiadhesion effects of PET and PMETM against *E. coli* for the indicated time. (C) Digital photographs of the antiadhesion effects of PET and PMETM against *B.subtilis* for the indicated time.

solution was added to each well and kept for 15 min. Next, the cells were carefully rinsed twice with PBS to wash away the unbound dye. Finally, fluorescence images were taken under a fluorescence microscope.

3. RESULTS AND DISCUSSION

3.1. Characterization of the Monomers and Polyester. The FTIR spectra of DEMT, DPMT, and PMETM are shown in Figure 1A. In terms of DEMT, absorption bands corresponding to the O-H and N-H stretching absorption and the $-CH_3$ stretching vibration of menthol (Figure 1A, black) could be observed at 3350 and 2953 cm^{-1}, respectively. Meanwhile, the absorption peak on behalf of the TCT (−C═N−) group was assigned at 1521 cm^{-1}. In terms of DPMT (Figure 1A, red), the absorption band corresponding to O-H and N-H stretching absorption could be observed at 3330 cm^{-1}. In addition, peaks at 1685 and 1310 cm^{-1} were assigned to the −C═O stretching vibration peak and the −C-O stretching vibration peak of the carboxyl group. The absorption peak at 1510 cm^{-1} was assigned to the O-H of carboxylic acid. In the FTIR spectra of PMETM (Figure 1A, blue), the presence of the ester functional group in polyester could be observed at 1718 cm^{-1}.

To further determine if the target polymer was successfully prepared, ^{1}H NMR spectrum was used to detect the characteristic functional groups of the polymer. Figure 1B displays the ^{1}H NMR spectra of DEMT, DPMT, and PMETM. In the ^{1}H NMR spectra of DEMT (Figure 1B, black), the distinct signals of aromatic protons of menthol appeared at δ = 0.70−2.08 ppm. The signals of peaks at 7.01 and 6.88 ppm correspond to the protons on the imino group, and the signals of peaks at 4.83, 3.46, and 3.33 ppm represent the protons of the hydroxyl group, methylene group adjacent to the hydroxyl group, and imino group, respectively. In terms of DPMT (Figure 1B, red), the resonance of aromatic protons appeared at 7.98 ppm, and the signals observed at 10.0 ppm were the protons of the imino group. The protons of the carboxylic acid group appeared at 12.3 ppm. In the ^{1}H NMR spectrum of PMETM (Figure 1B, blue), compared to DCMT and DPMT, the signals of the peak related to the hydroxyl group at 4.83 ppm and the carboxylic acid group at 12.3 ppm disappeared indicated that the esterification reaction between DEMT and DPMT took place.

The molecular weight and polydispersity index (PDI) of PMETM were determined by GPC (Table S1). The molecular weight of PMETM was 12 480 g/mol and the PDI value was 1.20, indicating the high molecular weight and the narrow distribution of the relative molecular mass of the polymer. This evidence proved that the required PMETM was synthesized successfully.

3.2. Bacterial Antiadhesion Assays. The antibacterial adhesion properties of PMETM were evaluated by the antibacterial spreading test and plate count experiments. The model for the visualized antibacterial spreading experiment is shown in Figure 2A. Figure 2B shows the evaluation of PET and PMETM for antiadhesion of Gram-negative *E. coli*. As shown in Figure 2B, within the first 24 h, *E. coli* managed to break the limits of PET and spread outward. Compared to PET, PMETM had a great restriction on the spread of *E. coli*, and after 120 h, *E. coli* could not break the restriction. Therefore, PMETM possesses an excellent ability to inhibit the growth of *E. coli*. In addition to this, Gram-positive *B. subtilis* was also used as a model bacterium to challenge PMETM to further assess the antibacterial ability of the material. As shown

https://doi.org/10.1021/acsbiomaterials.1c01448
ACS Biomater. Sci. Eng. XXXX, XXX, XXX−XXX

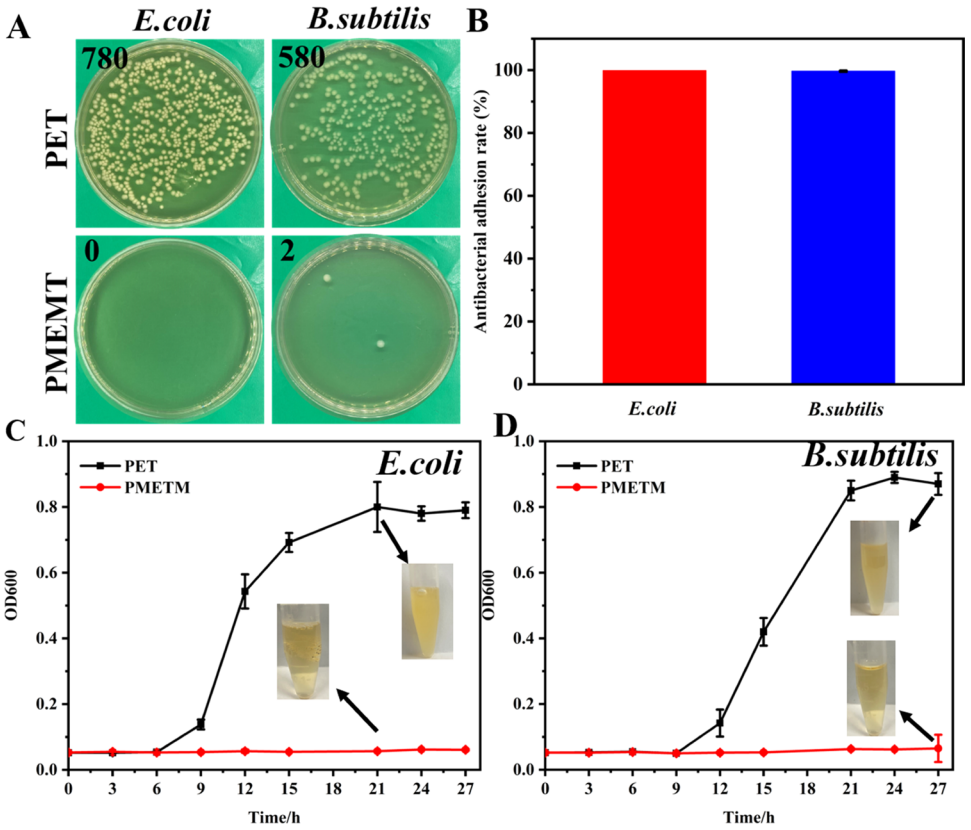

Figure 3. Quantitative antibacterial adhesion test of PMETM. (A) Plate count experiments of PET and PMETM against *E. coli* and *B. subtilis*. (B) Antibacterial adhesion rate of PET and PMETM against *E. coli* and *B. subtilis*. (C) Optical density 600 test results to evaluate the antibacterial properties of PET and PMETM against *E. coli* and *B. subtilis*.

in Figure 2C, after 24 h, *B. subtilis* broke through the PET material. A distinct bacterial ring could be observed on the surface of the medium. By contrast, PMETM was not broken until 120 h, indicating that PMETM effectively inhibited the growth of *B. subtilis*. As a result, PMETM has excellent capability against bacterial growth.

Further, the antiadhesive capacity of PMETM was quantified by the classical plate counting method. As shown in Figure 3A, after 24 h of contact with the bacterial suspension, the number of adherent *E. coli* colonies on PET was 780 units, while the number of adherent *E. coli* colonies on PMETM was 0 units. The number of *B. subtilis* colonies adhered to PET (580 units) was nearly 300 times higher than that of PMETM (2 units). In addition, the antibacterial adhesion rates of PMETM against *E. coli* and *B. subtilis* were 99.9 and 99.7%, respectively (Figure 3B), indicating that PMETM has excellent resistance to Gram-negative *E. coli* and Gram-positive *B. subtilis*. The optical density (OD) test was used to verify the above results. Figure 3C,D shows the OD test results obtained by incubating the bacteria adhering to the material surface in liquid medium for 27 h continuously. As shown in Figure 3C, after 6 h of incubation, the OD values of *E. coli* in the PET group began to show an increasing trend, indicating that *E. coli* began to enter the logarithmic growth phase. After 21 h of incubation, the OD of the bacterial suspension of the PET group reached the highest value and started to remain constant thereafter, indicating that *E. coli* entered a stable phase at this time. On the contrary, the OD of the PET group remained almost unchanged during the whole incubation process, indicating that there was almost no *E. coli* in the culture medium. After 21 h of incubation, the liquid medium of the PET group was able to be visualized showing a cloudy bacterial suspension (inset of Figure 3C), while the liquid medium of the PMETM group became suddenly transparent. This indicates that the *E. coli* adhering to the surface of the PET material far exceeded those adhering to the PMETM. As shown in Figure 3D, after 9 h of incubation, the OD value of *B. subtilis* in the PET group started to show an increasing trend, indicating that *B. subtilis* started to enter the logarithmic growth phase. After 21 h of incubation, the OD value of bacterial suspensions in the PET group reached the highest value and began to remain constant thereafter until 27 h, indicating that *B. subtilis* entered a stable phase at this time. By contrast, the OD values of the PMETM group did not increase significantly after 27 h of incubation. After 27 h of incubation, the liquid medium of the PET group was able to show a more turbid suspension of bacteria (inset of Figure 3D), while the liquid medium of the PMETM group remained clear. This indicates that less *B. subtilis* adhered to PMETM compared to PET.

3.3. Fungal Antiadhesion Assays. The antifungal adhesion ability of PMETM against *A. niger* was studied by the fungal landing test, as illustrated in Figure 4A. *A. niger* gradually started to grow and spread from the center. After 4 days, *A. niger* had gradually started to grow and spread on the PET surface, while the PMETM surface remained clean. After 30 days of incubation, this difference became more obvious. Further, a microscope was used to observe the attachment of spores on the PET and PMETM surfaces at the 30th day (Figure 4B). Figure 4C shows the morphology of the fungal cells attached to the above samples after 30 days of incubation.

https://doi.org/10.1021/acsbiomaterials.1c01448
ACS Biomater. Sci. Eng. XXXX, XXX, XXX−XXX

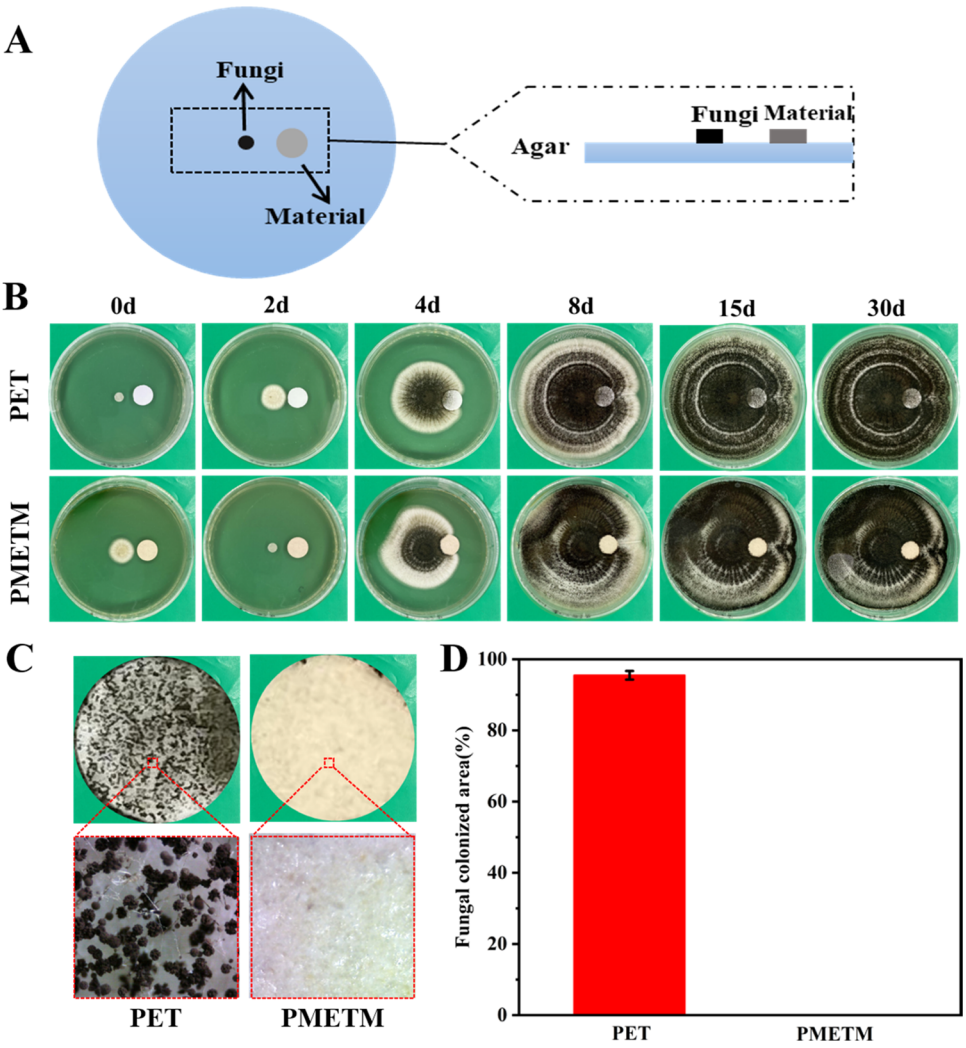

Figure 4. Fungal antiadhesion capability of PMETM. (A) Schematic illustration of the fungal landing test. (B) Digital photographs of the antiadhesion effects of PET and PMETM for the indicated days. (C) Enlarged images and micrographs of the antiadhesion effects of PET and PMETM at the 30th day. (D) Fungal colonized areas (%) of PET and PMETM.

The attachment of *A. niger* spores could be clearly seen on the PET surface, while the PMETM surface did not have any attachment of *A. niger* spores. The fungal coverage values of the surfaces of PET and PMETM were 95 and 0%, respectively (Figure 4D). In other words, PMETM could effectively prevent the adhesion and growth of *A. niger*. As a result, PMETM had excellent resistance to fungal adhesion and growth.

3.4. Mechanism of Microbial Antiadhesion. PMETM exhibited excellent antimicrobial (bacterial and fungal) adhesion capability through the insertion of menthoxytriazine in the skeleton of PET. The main reason is stereochemical modification of the polymer backbone using the menthoxy group, where the triazine group supplies a bridge. Menthol is a typical cyclic terpenoid with a stereochemical structure.[34] Microorganisms tend to avoid contact or adhesion with such terpenoid molecule-modified materials.[42] Based on the known reversible adhesion behavior of microorganisms to material surfaces, microorganisms could sense the stereochemical structure of menthoxy and respond to it. Microorganisms choose to avoid contact with the surface of the material. In other words, microorganisms do not choose to continue growing on the surface of the material.[25,43] Therefore, when the menthoxytriazine group was inserted into the PET backbone, the resulting PMETM exhibited good antimicrobial adhesion ability. Besides, the introduction of triazine groups enhances the complexity of the spatial structure of the polymer, which facilitates the exposure of menthoxy groups. Chemdraw software was used to simulate the spatial structures of PET and PMETM (Scheme 2A). It is noteworthy that the spatial structure of PET is a simple linear structure. By contrast, PMETM exhibits a more complex structure, where two adjacent menthoxy groups tend to approach each other because of hydrophobic interactions, forming a large hydrophobic cage-like structure. This is also proved by the results of the contact angle (CA) test (Scheme 2B). The presence of hydrophobic cage groups and exposure to the surface of the polymer make PMETM more hydrophobic than PET. In addition, PMETM did not produce a bacterial inhibition circle when interacting with *E. coli* and *B. subtilis* (Scheme 2C), indicating that PMETM did not achieve antiadhesive effects on microorganisms by releasing small molecules. All of the above illustrates that the antiadhesion of PMETM is achieved by the unique stereochemical structure of the menthoxy group.

3.5. Cytotoxicity Assays. Cytotoxicity is one of the most important evaluation criteria for the biocompatibility of

https://doi.org/10.1021/acsbiomaterials.1c01448
ACS Biomater. Sci. Eng. XXXX, XXX, XXX−XXX

Scheme 2. Schematic Representation of the Microbially Antiadhesive Effect[a]

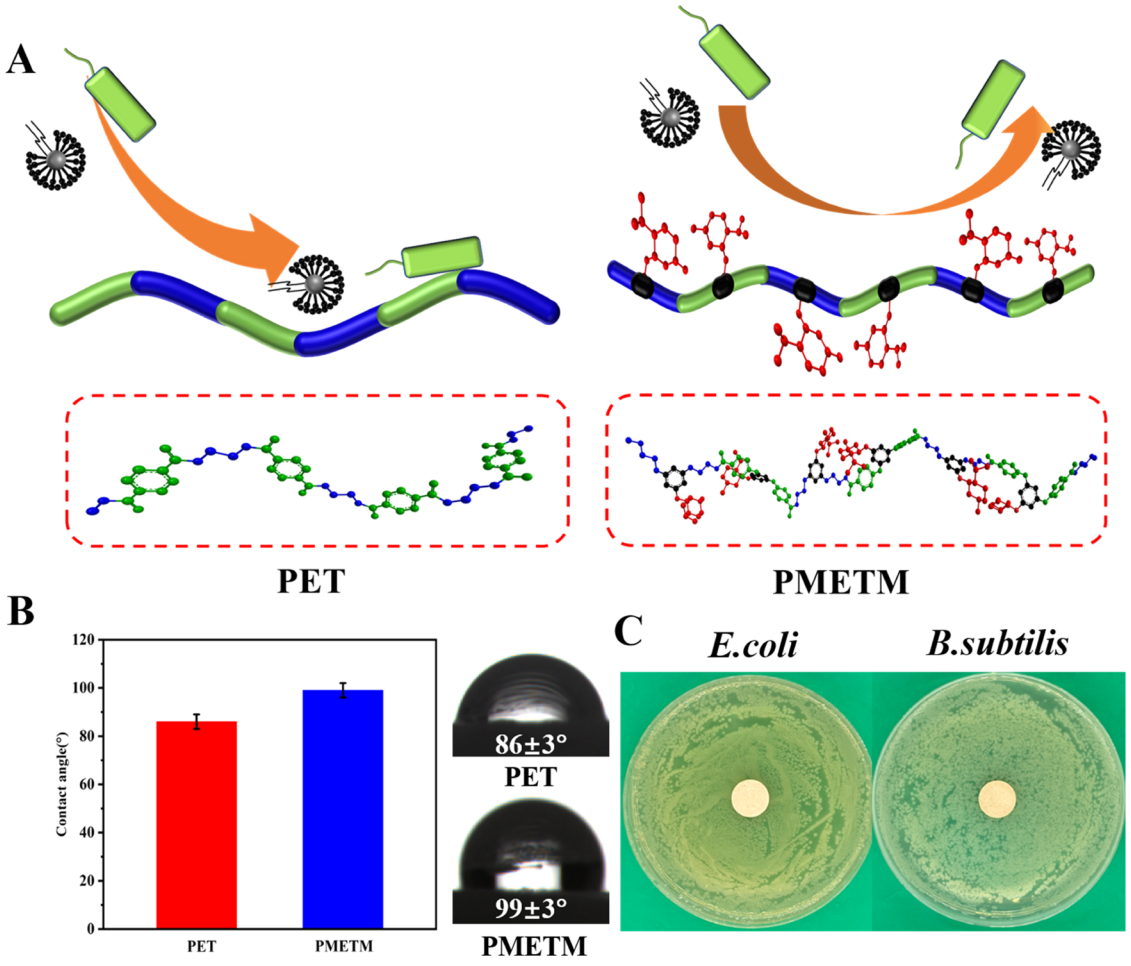

[a](A) Antimicrobial adhesion mechanism of PMETM. (B) Contact angles of PET and PMETM. (C) Inhibition zone test of PMETM against *E. coli* and *S. aureus*.

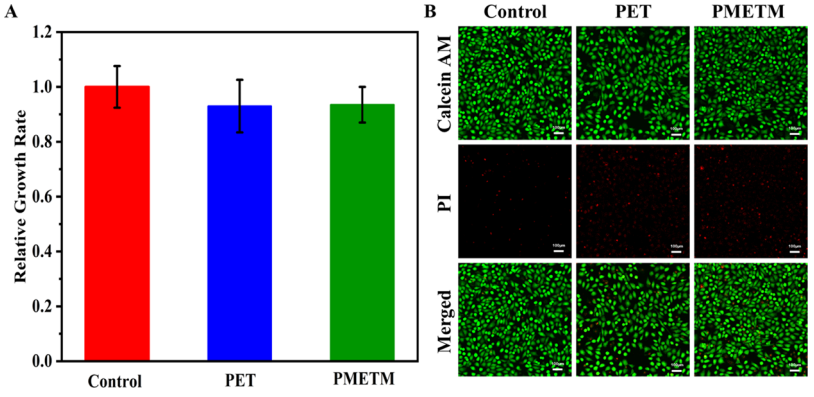

Figure 5. Cytotoxicity assays of PMETM. (A) MTT results of the relative growth rates (RGR) in L929 cells after 48 h of incubation with the corresponding PET and PMETM conditioned medium. (B) Fluorescence microscopy images of L929 cells after treatment with PET and PMETM after 48 h of incubation.

antimicrobial materials. Therefore, the MTT assay was used to confirm the cytotoxicity of PMETM. The relative growth rates (RGRs) of PET and PMETM on L929 cells are shown in Figure 5A. After 48 h of incubation, the RGRs of PET and PMETM were 93.0 ± 9.6 and 93.5 ± 6.5%, respectively. According to the standard toxicity rating, the cytotoxicity of PMETM was in grade 1. Fluorescence microscopy imaging was used to further confirm cell viability. Figure 5B shows the image of L929 cells observed under green and red filters after double staining with calcein AM and ethylenediamine homodimer. Green spots indicated living cells, while red spots represented dead cells with damaged membranes. As can be seen from the image, L929 cells in both PET and PMETM groups exhibited high viability. Thus, PMETM is an antimicrobial material without cytotoxicity.

https://doi.org/10.1021/acsbiomaterials.1c01448
ACS Biomater. Sci. Eng. XXXX, XXX, XXX−XXX

4. CONCLUSIONS

In summary, PMETM, a novel antimicrobial PET polymer containing double menthoxytriazine, was synthesized by polycondensation between DEMT and DPMT. This polymer had good antimicrobial adhesion properties with 99.9 and 99.7% antiadhesion rate against *E. coli* and *B. subtilis*, respectively, and resistance to coverage in *A. niger* within 30 days. The insertion of double menthoxytriazine groups ensured the inhibition of PMETM against harmful microorganisms. In addition, PMETM was a noncytotoxic material, making it a highly promising antiadhesive polymer. Therefore, this strategy for the antimicrobial modification of PET by inserting antimicrobial triazine derivatives into the PET backbone was feasible. Although menthol was used as an antimicrobial unit, it is clear that other types of small molecules (e.g., quaternary ammonium salt, *N*-haloamines, etc.) can also be used to achieve antimicrobial modification of PET for upgrading using the same strategy.

■ ASSOCIATED CONTENT

Supporting Information

The Supporting Information is available free of charge at https://pubs.acs.org/doi/10.1021/acsbiomaterials.1c01448.

^{1}H NMR spectra of monomers and polymers and the GPC and MTT results of PMETM (PDF)

■ AUTHOR INFORMATION

Corresponding Author

Xing Wang − *Beijing Laboratory of Biomedical Materials, College of Life Science and Technology, Beijing University of Chemical Technology, Beijing 100029, P. R. China;* orcid.org/0000-0002-9990-1479; Email: wangxing@mail.buct.edu.cn

Authors

Pengfei Zhang − *Beijing Laboratory of Biomedical Materials, College of Life Science and Technology, Beijing University of Chemical Technology, Beijing 100029, P. R. China*

Jiyu Li − *Beijing Laboratory of Biomedical Materials, College of Life Science and Technology, Beijing University of Chemical Technology, Beijing 100029, P. R. China*

Mei Yang − *Beijing Laboratory of Biomedical Materials, College of Life Science and Technology, Beijing University of Chemical Technology, Beijing 100029, P. R. China*

Lifei Huang − *Beijing Laboratory of Biomedical Materials, College of Life Science and Technology, Beijing University of Chemical Technology, Beijing 100029, P. R. China*

Fanqiang Bu − *Beijing Laboratory of Biomedical Materials, College of Life Science and Technology, Beijing University of Chemical Technology, Beijing 100029, P. R. China*

Zixu Xie − *Beijing Laboratory of Biomedical Materials, College of Life Science and Technology, Beijing University of Chemical Technology, Beijing 100029, P. R. China*

Guofeng Li − *Beijing Laboratory of Biomedical Materials, College of Life Science and Technology, Beijing University of Chemical Technology, Beijing 100029, P. R. China*

Complete contact information is available at: https://pubs.acs.org/10.1021/acsbiomaterials.1c01448

Notes

The authors declare no competing financial interest.

■ ACKNOWLEDGMENTS

The authors thank the National Natural Science Foundation of China (21574008) and the Fundamental Research Funds for the Central Universities of China (BHYC1705B) for their financial support.

■ REFERENCES

(1) Kumar, S.; Roy, D. N.; Dey, V. A Comprehensive Review on Techniques to Create the Anti-Microbial Surface of Biomaterials to Intervene in Biofouling. *Colloid Interface Sci. Commun.* **2021**, *43*, No. 100464.

(2) Thongsong, W.; Kulsetthanchalee, C.; Threepopnatkul, P. Effect of Polybutylene Adipate-Co-Terephthalate on Properties of Polyethylene Terephthalate Thin Films. *Mater. Today: Proc.* **2017**, *4*, 6597−6604.

(3) Ding, L.; Liu, L.; Chen, Y. F.; Du, Y.; Guan, S. J.; Bai, Y.; Huang, Y. Modification of Poly(Ethylene Terephthalate) by Copolymerization of Plant-Derived A-Truxillic Acid with Excellent Ultraviolet Shielding and Mechanical Properties. *Chem. Eng. J.* **2019**, *374*, 1317−1325.

(4) Zhang, C.; Li, Y.; Ma, C.; Zhang, Q. Recent Progress of Organic−Inorganic Hybrid Perovskites in RRAM, Artificial Synapse, and Logic Operation. *Small Sci.* **2021**, No. 2100086.

(5) Ping, X.; Wang, M.; Xuewu, G. Surface Modification of Poly(Ethylene Terephthalate) (PET) Film by Gamma-Ray Induced Grafting of Poly(Acrylic Acid) and Its Application in Antibacterial Hybrid Film. *Radiat. Phys. Chem.* **2011**, *80*, 567−572.

(6) Yu, Y.; Bu, F.; Zhou, H.; Wang, Y.; Cui, J.; Wang, X.; Nie, G.; Xiao, H. Biosafety Materials: An Emerging New Research Direction of Materials Science from the COVID-19 Outbreak. *Mater. Chem. Front.* **2020**, *4*, 1930−1953.

(7) Mallakpour, S.; Azadi, E.; Hussain, C. M. Recent Breakthroughs of Antibacterial and Antiviral Protective Polymeric Materials during COVID-19 Pandemic and after Pandemic: Coating, Packaging, and Textile Applications. *Curr. Opin. Colloid Interface Sci.* **2021**, *55*, No. 101480.

(8) Zheng, Z.; Guo, J.; Mao, H.; Xu, Q.; Qin, J.; Yan, F. Metal-Containing Poly(Ionic Liquid) Membranes for Antibacterial Applications. *ACS Biomater. Sci. Eng.* **2017**, *3*, 922−928.

(9) Bai, R.; Kang, J.; Simalou, O.; Liu, W.; Ren, H.; Gao, T.; Gao, Y.; Chen, W.; Dong, A.; Jia, R. Novel N−Br Bond-Containing N-Halamine Nanofibers with Antibacterial Activities. *ACS Biomater. Sci. Eng.* **2018**, *4*, 2193−2202.

(10) Zou, Y.; Lu, K.; Lin, Y.; Wu, Y.; Wang, Y.; Li, L.; Huang, C.; Zhang, Y.; Brash, J. L.; Chen, H.; Yu, Q. Dual-Functional Surfaces Based on an Antifouling Polymer and a Natural Antibiofilm Molecule: Prevention of Biofilm Formation without Using Biocides. *ACS Appl. Mater. Interfaces* **2021**, *13*, 45191−45200.

(11) Zhou, J.; Fei, X.; Li, C.; Yu, S.; Hu, Z.; Xiang, H.; Sun, B.; Zhu, M. Integrating Nano-Cu2O@ZrP into In Situ Polymerized Polyethylene Terephthalate (PET) Fibers with Enhanced Mechanical Properties and Antibacterial Activities. *Polymers* **2019**, *11*, No. 113.

(12) Xin, X.; Li, P.; Zhu, Y.; Shi, L.; Yuan, J.; Shen, J. Mussel-Inspired Surface Functionalization of PET with Zwitterions and Silver Nanoparticles for the Dual-Enhanced Antifouling and Antibacterial Properties. *Langmuir* **2019**, *35*, 1788−1797.

(13) Bao, Q.; Nishimura, N.; Kamata, H.; Furue, K.; Ono, Y.; Hosomi, M.; Terada, A. Antibacterial and Anti-Biofilm Efficacy of Fluoropolymer Coating by a 2,3,5,6-Tetrafluoro-p-Phenylenedimethanol Structure. *Colloids Surf., B* **2017**, *151*, 363−371.

(14) Zhang, S.; Li, R.; Huang, D.; Ren, X.; Huang, T. S. Antibacterial Modification of PET with Quaternary Ammonium Salt and Silver Particles via Electron-Beam Irradiation. *Mater. Sci. Eng., C* **2018**, *85*, 123−129.

(15) Naeem, M.; Felipe, M. B. M. C.; de Medeiros, S. R. B.; Costa, T. H. C.; Libório, M. S.; Alves, C.; Nascimento, R. M.; Nascimento, I. O.; Sousa, R. R. M.; Feitor, M. C. Novel Antibacterial Silver Coating

on PET Fabric Assisted with Hollow-Cathode Glow Discharge. *Polym. Adv. Technol.* **2020**, *31*, 2896−2905.
(16) Chai, D.; Liu, W.; Hao, X.; Wang, H.; Wang, H.; Hao, Y.; Gao, Y.; Qu, H.; Wang, L.; Dong, A.; Gao, G. Mussel-Inspired Synthesis of Magnetic N-Halamine Nanoparticles for Antibacterial Recycling. *Colloid Interface Sci. Commun.* **2020**, *39*, No. 100320.
(17) Huang, W.; Tao, F.; Li, F.; Mortimer, M.; Guo, L. H. Antibacterial Nanomaterials for Environmental and Consumer Product Applications. *NanoImpact* **2020**, *20*, No. 100268.
(18) Azizi Lalabadi, M.; Garavand, F.; Jafari, S. M. Incorporation of Silver Nanoparticles into Active Antimicrobial Nanocomposites: Release Behavior, Analyzing Techniques, Applications and Safety Issues. *Adv. Colloid Interface Sci.* **2021**, *293*, No. 102440.
(19) Huang, J. Y.; Li, X.; Zhou, W. Safety Assessment of Nanocomposite for Food Packaging Application. *Trends Food Sci. Technol.* **2015**, *45*, 187−199.
(20) Mei, L.; Zhang, X.; Wang, Y.; Zhang, W.; Lu, Z.; Luo, Y.; Zhao, Y.; Li, C. Multivalent Polymer−Au Nanocomposites with Cationic Surfaces Displaying Enhanced Antimicrobial Activity. *Polym. Chem.* **2014**, *5*, 3038−3044.
(21) Das, C. G. A.; Kumar, V. G.; Dhas, T. S.; Karthick, V.; Govindaraju, K.; Joselin, J. M.; Baalamurugan, J. Antibacterial Activity of Silver Nanoparticles (Biosynthesis): A Short Review on Recent Advances. *Biocatal. Agric. Biotechnol.* **2020**, *27*, No. 101593.
(22) Li, K.; Chen, J.; Xue, Y.; Ding, T.; Zhu, S.; Mao, M.; Zhang, L.; Han, Y. Polymer Brush Grafted Antimicrobial Peptide on Hydroxyapatite Nanorods for Highly Effective Antibacterial Performance. *Chem. Eng. J.* **2021**, *423*, No. 130133.
(23) Wei, T.; Yu, Q.; Chen, H. Responsive and Synergistic Antibacterial Coatings: Fighting against Bacteria in a Smart and Effective Way. *Adv. Healthcare Mater.* **2019**, *8*, No. 1801381.
(24) Zou, Y.; Zhang, Y.; Yu, Q.; Chen, H. Dual-Function Antibacterial Surfaces to Resist and Kill Bacteria: Painting a Picture with Two Brushes Simultaneously. *J. Mater. Sci. Technol.* **2021**, *70*, 24−38.
(25) Li, G.; Zhao, H.; Hong, J.; Quan, K.; Yuan, Q.; Wang, X. Antifungal Graphene Oxide-Borneol Composite. *Colloids Surf., B* **2017**, *160*, 220−227.
(26) Xin, Y.; Zhao, H.; Xu, J.; Xie, Z.; Li, G.; Gan, Z.; Wang, X. Borneol-Modified Chitosan: Antimicrobial Adhesion Properties and Application in Skin Flora Protection. *Carbohydr. Polym.* **2020**, *228*, No. 115378.
(27) Yang, L.; Zhan, C.; Huang, X.; Hong, L.; Fang, L.; Wang, W.; Su, J. Durable Antibacterial Cotton Fabrics Based on Natural Borneol-Derived Anti-MRSA Agents. *Adv. Healthcare Mater.* **2020**, *9*, No. 2000186.
(28) Zhang, L.; Ma, Z.; Wang, R.; Zhu, M. Synthesis and Characterization of Methacrylate-Functionalized Betulin Derivatives as Antibacterial Comonomer for Dental Restorative Resins. *ACS Biomater. Sci. Eng.* **2021**, *7*, 3132−3140.
(29) Hu, J.; Sun, B.; Zhang, H.; Lu, A.; Zhang, H.; Zhang, H. Terpolymer Resin Containing Bioinspired Borneol and Controlled Release of Camphor: Synthesis and Antifouling Coating Application. *Sci. Rep.* **2020**, *10*, No. 10375.
(30) Cheng, Q.; Asha, A. B.; Liu, Y.; Peng, Y. Y.; Diaz Dussan, D.; Shi, Z.; Cui, Z.; Narain, R. Antifouling and Antibacterial Polymer-Coated Surfaces Based on the Combined Effect of Zwitterions and the Natural Borneol. *ACS Appl. Mater. Interfaces* **2021**, *13*, 9006−9014.
(31) Song, F.; Zhang, L.; Chen, R.; Liu, Q.; Liu, J.; Yu, J.; Liu, P.; Duan, J.; Wang, J. Bioinspired Durable Antibacterial and Antifouling Coatings Based on Borneol Fluorinated Polymers: Demonstrating Direct Evidence of Antiadhesion. *ACS Appl. Mater. Interfaces* **2021**, *13*, 33417−33426.
(32) Wang, X.; Jing, S.; Liu, Y.; Liu, S.; Tan, Y. Diblock Copolymer Containing Bioinspired Borneol and Dopamine Moieties: Synthesis and Antibacterial Coating Applications. *Polymer* **2017**, *116*, 314−323.
(33) Wu, J.; Wang, C.; Mu, C.; Lin, W. A Waterborne Polyurethane Coating Functionalized by Isobornyl with Enhanced Antibacterial Adhesion and Hydrophobic Property. *Eur. Polym. J.* **2018**, *108*, 498−506.
(34) Xu, J.; Xie, Z.; Du, F.; Wang, X. One-Step Anti-Superbug Finishing of Cotton Textiles with Dopamine-Menthol. *J. Mater. Sci. Technol.* **2021**, *69*, 79−88.
(35) Li, X.; Xie, Z.; Li, G.; Tao, L.; Wei, Y.; Wang, X. Antifungal Polymer Containing Menthoxy Triazine. *ACS Appl. Polym. Mater.* **2021**, 3702.
(36) Kamatou, G. P. P.; Vermaak, I.; Viljoen, A. M.; Lawrence, B. M. Menthol: A Simple Monoterpene with Remarkable Biological Properties. *Phytochemistry* **2013**, *96*, 15−25.
(37) Hollink, E.; Simanek, E. E.; Bergbreiter, D. E. Strategies for Protecting and Manipulating Triazine Derivatives. *Tetrahedron Lett.* **2005**, *46*, 2005−2008.
(38) Chouai, A.; Simanek, E. E. Kilogram-Scale Synthesis of a Second-Generation Dendrimer Based on 1,3,5-Triazine Using Green and Industrially Compatible Methods with a Single Chromatographic Step. *J. Org. Chem.* **2008**, *73*, 2357−2366.
(39) Chamsaz, E. A.; Mankoci, S.; Barton, H. A.; Joy, A. Nontoxic Cationic Coumarin Polyester Coatings Prevent Pseudomonas Aeruginosa Biofilm Formation. *ACS Appl. Mater. Interfaces* **2017**, *9*, 6704−6711.
(40) Sun, X.; Qian, Z.; Luo, L.; Yuan, Q.; Guo, X.; Tao, L.; Wei, Y.; Wang, X. Antibacterial Adhesion of Poly(Methyl Methacrylate) Modified by Borneol Acrylate. *ACS Appl. Mater. Interfaces* **2016**, *8*, 28522−28528.
(41) Chen, C.; Xie, Z.; Zhang, P.; Liu, Y.; Wang, X. Cooperative Enhancement of Fungal Repelling Performance by Surface Photografting of Stereochemical Bi-Molecules. *Colloids Interface Sci. Commun.* **2021**, *40*, No. 100336.
(42) Hook, A. L.; Chang, C. Y.; Yang, J.; Luckett, J.; Cockayne, A.; Atkinson, S.; Mei, Y.; Bayston, R.; Irvine, D. J.; Langer, R.; Anderson, D. G.; Williams, P.; Davies, M. C.; Alexander, M. R. Combinatorial Discovery of Polymers Resistant to Bacterial Attachment. *Nat. Biotechnol.* **2012**, *30*, 868−875.
(43) Ma, Y.; Shi, L.; Yue, H.; Gao, X. Recognition at Chiral Interfaces: From Molecules to Cells. *Colloids Surf., B* **2020**, *195*, No. 111268.

https://doi.org/10.1021/acsbiomaterials.1c01448
ACS Biomater. Sci. Eng. XXXX, XXX, XXX−XXX